C Journal of Carbon Research

MDPI

Article

Pull-Out of Pristine and Functionalized Carbon Nanotubes from Cement: A Molecular Modelling Study

Isabel Lado-Touriño

Engineering Department, School of Architecture, Engineering and Design, Universidad Europea de Madrid, 28760 Villaviciosa de Odón, Spain; misabel.lado@universidadeuropea.es

Abstract: Carbon nanotubes (CNTs) are widely used as reinforcements in cement-based composites. The improvement in the mechanical properties of the resulting materials depends on the characteristics of the interface formed between CNTs and the cement matrix. The experimental characterization of the interfacial properties of these composites is still limited and hard to achieve with currently available technologies. In this work, molecular dynamics and molecular mechanics pull-out simulations of pristine and functionalized CNTs, taken from a tobermorite crystal, were carried out to study interfacial shear strength (ISS) from an atomic perspective. ISS was calculated from the potential energy of the systems. The effects of the CNT diameter and the degree of functionalization on the pull-out process were analyzed according to the ISS and non-bonded energy results. The influence of H-bonding and electrostatic interactions between the CNT and the matrix were also studied. The results show that ISS decreases with increasing CNT radius for pristine CNTs and depends upon the number of H-bonds for functionalized CNTs. ISS values are positively correlated to $E_{\text{non-bonded energy}}$, which is related to the number of carboxyl groups on the CNT surface. A high degree of functionalization increases both the number of H-bonds and the number of Ca^{2+}-O interactions between the CNT and the tobermorite surface. This results in a stronger interfacial interaction and, therefore, an elevated ISS value.

Keywords: carbon nanotubes; cement; molecular mechanics; molecular dynamics; pull-out; interfacial shear strength

Citation: Lado-Touriño, I. Pull-Out of Pristine and Functionalized Carbon Nanotubes from Cement: A Molecular Modelling Study. *C* **2022**, *8*, 80. https://doi.org/10.3390/c8040080

Academic Editor: Gil Gonçalves

Received: 21 November 2022
Accepted: 13 December 2022
Published: 16 December 2022

1. Introduction

Cementitious composites are widely used materials with high compressive strength and simple production methods. However, they also have many disadvantages such as low tensile strength, high permeability to water and other harmful substances, and high cracking tendency. Reinforcements are used to overcome these drawbacks. Due to their remarkable mechanical properties, carbon nanotubes (CNTs) are promising candidates as reinforcing materials. During the last few years, there have been an increasing number of research studies on composites made of cement and CNTs [1–5]. Mechanical testing has shown that CNTs have elastic moduli greater than 1 TPa and tensile strengths as high as 63 GPa [6,7]. When appropriate dispersion of CNTs within the cement matrix is achieved, the resulting composites show denser structures [8], reduced water permeability [9], improved mechanical properties [10] and good durability [11]. The improved mechanical properties are attributed to the crack-bridging effect of CNTs. The addition of CNTs to a cement matrix results in a delay in cracks propagation. A recent study [12] shows that the use of functionalized CNTs improves compressive strength of cement pastes without the need for ultrasonication. Thus, good dispersion of the reinforcement into the matrix and improved interfacial interactions, enhanced by the functional groups, are the key factors in obtaining materials with better properties. CNTs have also been used as additives to enhance the bonding strength between concrete- and carbon fiber-reinforced polymers [13],

which in turn increased the bond strength, ultimate slip, and interfacial fracture energy of the composites.

It is well known that the interface between CNTs and the cement matrix plays a critical role in determining the effectiveness of mechanical reinforcement, as the interface is usually the weakest part in a composite and determines its fracture behavior [14]. Apart from diverse experimental results, recent coarse-grained and all-atoms molecular dynamics studies [15,16] suggest that the addition of CNT to a cement matrix changes the way of fracturing and significantly improves the fracture energy and other mechanical properties.

Interfacial bond strength can be tailored in many ways, one of which is functionalizing the CNT surface [17,18]. The functionalization processes can be classified into two broad groups depending on the nature of the interactions established between the CNTs and the molecules linked to them [19]: covalent functionalization, which implies the formation of strong chemical bonds between the CNTs and the functional groups, and non-covalent functionalization, which is based on different adsorption forces (hydrogen bonds, van der Waals forces, electrostatic forces or π-stacking interactions) and does not modify the properties of CNTs [20]. Non-covalent functionalization is weaker than covalent functionalization, which may result in low efficiency of the load transfer in composites [21]. Acid treatment of the CNTs allows for covalent modification and is commonly used to introduce carboxyl groups to the sidewalls of CNTs [22], thereby facilitating dispersion as well as improving the bonding between CNTs and the cement matrix [23,24].

A direct measure of the interfacial bond strength can be estimated from the interfacial shear strength (ISS), which can be obtained from micromechanical and macromechanical tests, such as fragmentation, pull-out, microdroplet, push-out and push-in tests [25–30]. A consensus is yet to emerge on the best experimental technique to measure the ISS, and most experimental studies have focused on CNTs-reinforced polymer composites.

Due to the difficulties in obtaining experimental results to study the CNT–cement interface, the interfacial properties of CNTs-reinforced cementitious composites have mainly been studied by molecular mechanics (MM) and molecular dynamics (MD) simulations. It is important to note that this kind of simulations can take advantage of providing atomic information of the interface between CNTs and matrices, which is unattainable with experimental methods. Many authors have calculated ISS using a pull-out model [31]. This is because the CNT–matrix interface strength is essentially related to the pulling-out behavior, which determines how strongly the CNT is bonded to the matrix, and how effective the reinforcement is. As in the case of experimental results, ISS of CNTs-reinforced polymer composites has been extensively studied by molecular modelling [32–36], and only several results on carbonaceous nanomaterials–cement matrices have been reported in the literature, most of which related to graphene [37–40]. As the interface between CNTs and matrices play a critical role in enhancing the mechanical properties of the composites, the influence of the functionalization of the CNT surface on the pull-out process has also been studied by many authors [40–45]. Both simulation and experimental results show that cement composites, containing functionalized CNTs, result in improved mechanical properties due to a better adhesion at the interface. However, technical difficulties associated with the manipulation of the nanotubes in cement matrices, hinder the measurement of ISS of these composites.

After carrying out a review of the existing literature, we noticed that there are many experimental results on ISS of CNT-containing composites, but most of them have focused on polymeric matrices, as ISS of CNT–cement composites are difficult to measure experimentally. On the other hand, simulation studies of cementitious composites are more numerous, especially those that contain graphene and graphene-derived reinforcements. There are some MD calculations of mechanical properties of CNT–cement composites, but almost none focuses on ISS of functionalized CNTs. Therefore, in this work, the ISS of CNT/tobermorite nanocomposites was systematically studied by using a series of CNT pull-out simulations based on MD and MM approaches. The results are explained as a function of non-bonded energies, which in turn, are influenced by the chemical interactions

established between the CNTs and the matrix at the composite interface. Pristine and functionalized armchair CNTs, with a radius in the range of 2.70 to 4.74 Å and a length of 19.68 Å, were inserted into a tobermorite matrix. The effect of CNT diameter and degree of functionalization with carboxyl groups on ISS was assessed and related to non-bonded interactions between the CNT and the matrix. To the best of our knowledge, molecular simulations of a CNT pull-out from a cement matrix, unlike in the case of polymer matrices or graphene, are scarce. With this work, we are aiming to get more insight into the atomic interactions existing at CNT–cement interfaces, which are primarily responsible for the enhancements and failures of the mechanical properties of these composites.

2. Materials and Methods

2.1. Model Systems

A simulation cell, with a periodic boundary condition in the y–z plane (29.54 × 67.46 Å^2), was used for the pull-out calculations. The size of this cell was large enough (500 Å) in the axial direction of the CNT (*x* direction), and included a vacuum layer to eliminate the interaction between periodic images in neighboring cells and leave space for pulling out the CNT (Figure 1).

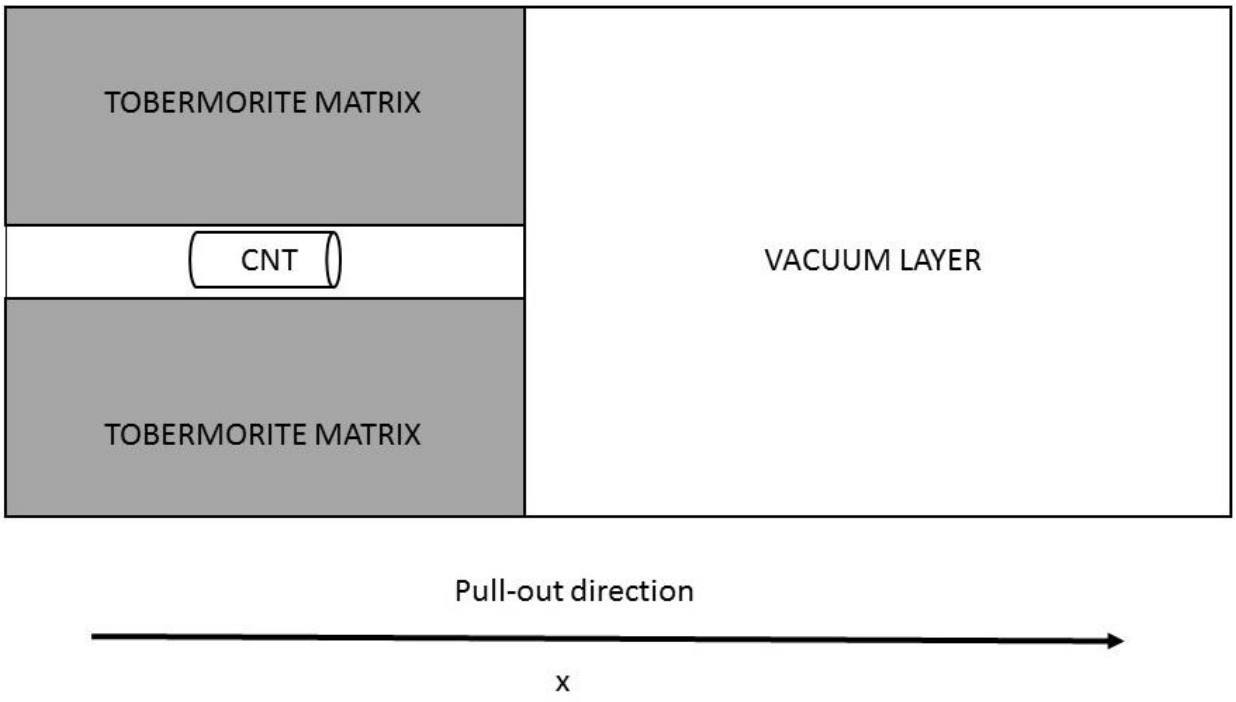

Figure 1. Schematic cell for the pull-out simulations.

To represent the cement matrix, a tobermorite 11 Å structure was used (left side of Figure 2). This structure contained double silicon oxide chains interspersed with calcium oxide sheets and hydration water molecules; 11 Å indicates the basal spacing of the calcium oxide layers. Although it is well known that real cementitious systems present poor crystalline order with variable stoichiometry [46], tobermorite has been regarded as a good model of cement structures by many different authors [47–49].

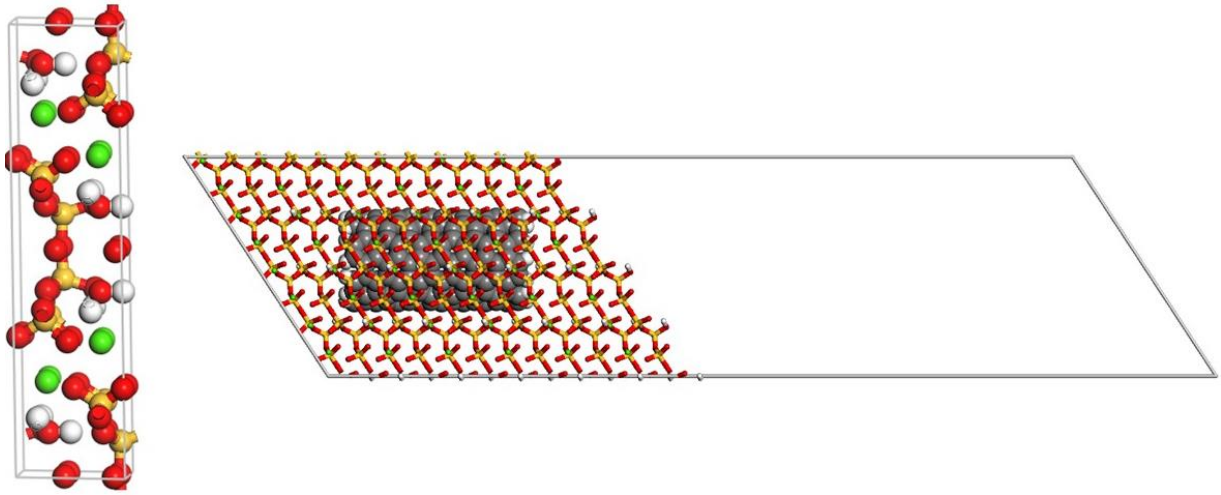

Figure 2. Tobermorite crystal (**left**) and top view of a tobermorite/CNT composite (**right**).

Since the interface between the tobermorite and the CNT is the focus of this research, we think this model is reasonable and can work well for our purposes.

The composite material was built by inserting a CNT into the tobermorite matrix (right side of Figure 2). CNTs with radius ranging from 2.71 to 4.74 Å (CNT (4, 4) = 2.70 Å, CNT (5, 5) = 3.39 Å, CNT (6, 6) = 4.07 Å and CNT (7, 7) = 4.74 Å) and a length of 19.68 Å, functionalized with different numbers of carboxyl groups (0, 2, 4, 6 and 10), were used to study the influence of diameter and degree of functionalization on ISS. The geometrical characteristics of the CNTs are presented in Table 1, and a few representative examples of the CNTs used for the simulations are shown in Figure 3.

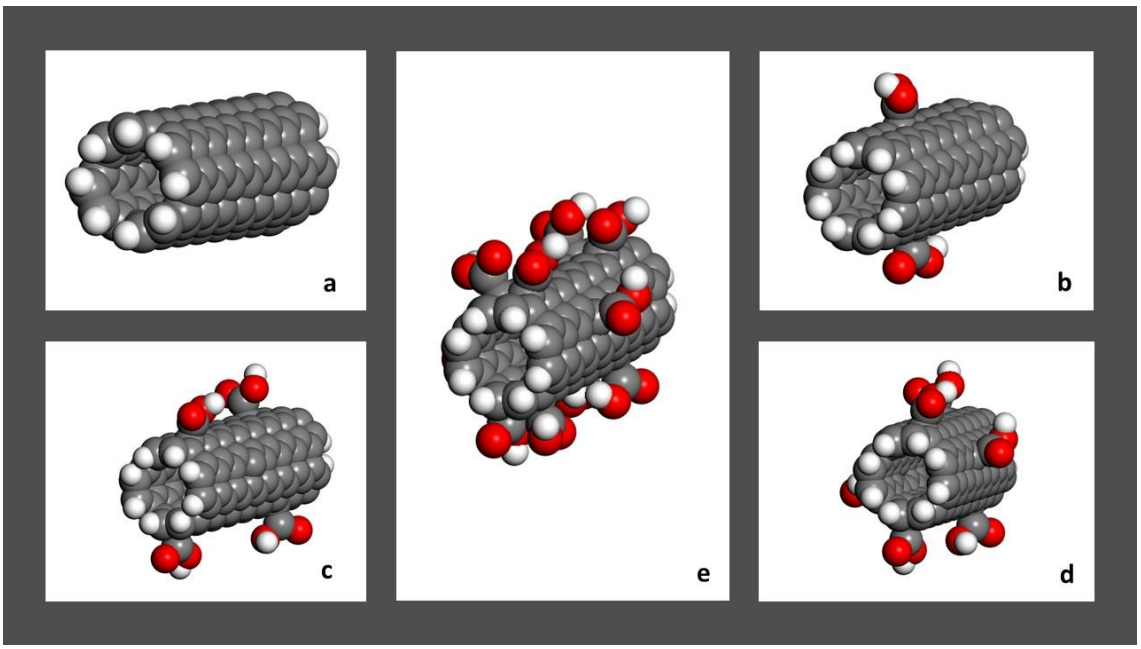

Figure 3. Pristine (**a**) and functionalized CNTs: 2 COOH (**b**), 4 COOH (**c**), 6 COOH (**d**) and 10 COOH (**e**).

Table 1. Geometrical characteristics of the CNTs used in the simulations.

System	Radius (Å)	Length (Å)	Number of COOH Groups
CNT (4, 4)	2.71		0
CNT (5, 5)	3.39		2
CNT (6, 6)	4.07	9.84	4
CNT (7, 7)	4.74		10

2.2. Calculation Method

Initially, a 100 ps calculation in the NPT ensemble at 298 K and atmospheric pressure was performed to optimize the parameters of the simulation lattice and relax the system. The temperature was controlled by a Nose–Hoover thermostat [50], and a Berendsen barostat [51] was used to maintain the pressure at 1 atm. A time step of 1 fs was used during the entire relaxation. Then, the resulting relaxed structures were used as inputs to simulate the pull-out process. This was done after increasing the size of the cell in the axial direction of the CNT (x direction) and including a vacuum layer, while keeping the lattice parameters in the other two directions unchanged. These new models were further optimized by molecular mechanics (MM) before the pull-out process. The models used to simulate the pull-out process were created by displacing the CNT along the x axis in increments of 10 Å. Snapshots of the models for one of the CNT/tobermorite systems during the CNT pull-out process are shown in Figure 4. After each pull-out step, the energy of the resulting molecular structure was calculated by MM. Materials Studio 9.0 software [52] was used to perform the simulations.

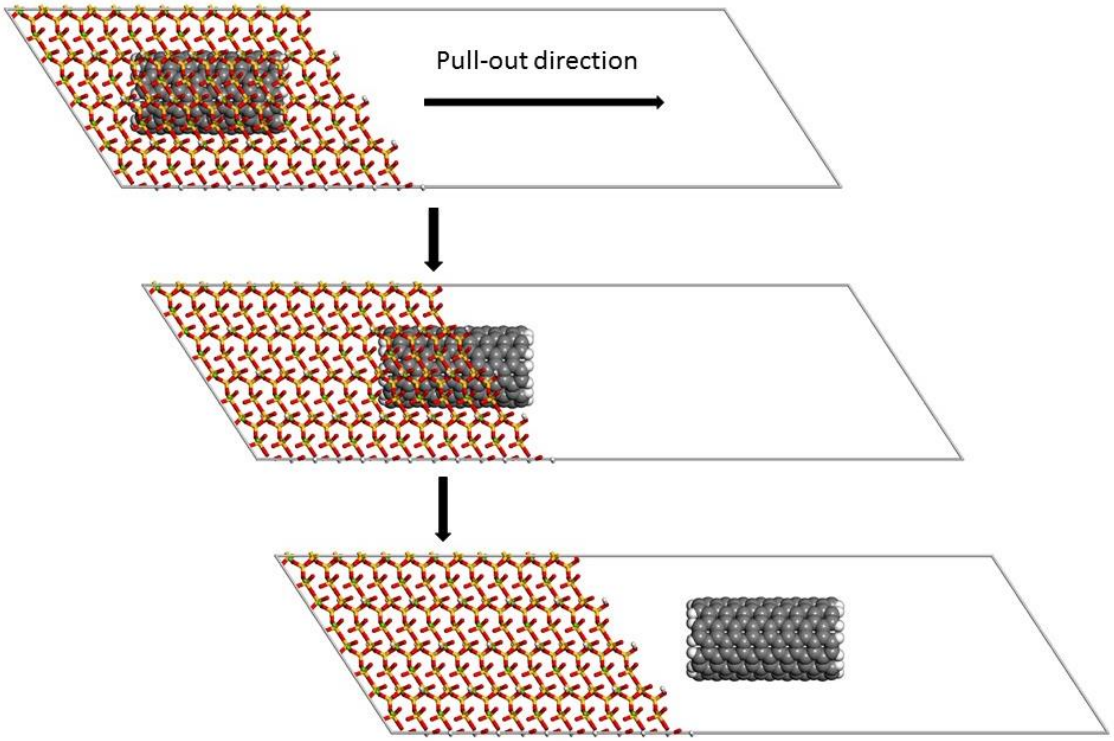

Figure 4. Snapshots of the pull-out process in the CNT/tobermorite composites.

The COMPASSII force field was used to calculate the interactions between the tobermorite and the CNT [53]. COMPASSII has been successfully applied in the simulation of systems containing CNTs and different materials derived from cement [38,54–57]. Coulomb interactions were calculated by the Ewald summation method, and an atom-based cut-

off method was applied for the calculation of van der Waal interactions [58]. The cutoff distance for both kind of interactions was set to 12.5 Å.

The interfacial shear strength (ISS = τ) was calculated based on the total pull-out energy, and is given by [59]:

$$\tau = \frac{E_{pull\text{-}out}}{\pi\, r\, L^2} \quad (1)$$

τ, r, and L are the interfacial shear strength, CNT radius and CNT length. $E_{pull\text{-}out}$ is the energy difference between the fully embedded configuration of the CNT and the complete pull-out configuration (see Figure 5). It should be noted that this formula gives the average ISS.

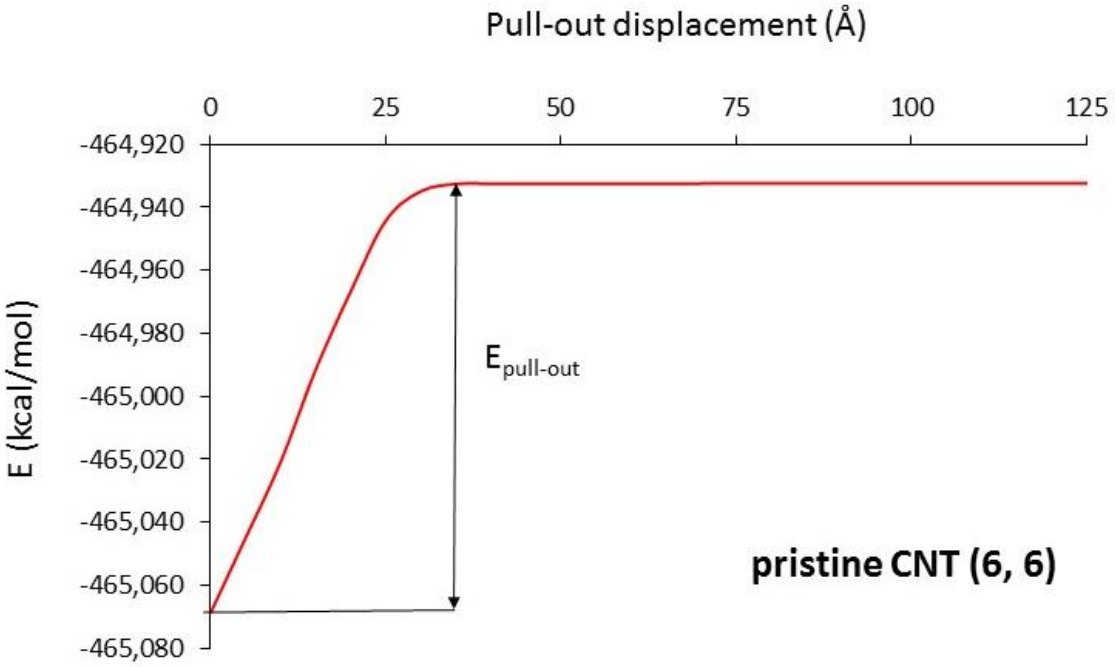

Figure 5. Variation of total potential energy with pull-out displacement.

3. Results and Discussion

3.1. Interfacial Shear Strength

Figure 5 shows the variation in total potential energy of the composite, with pull-out displacement for one of the models. As the CNT was pull out from the tobermorite matrix, the total potential energy increased toward a constant value, which indicated that there was no interaction between the CNT and the matrix beyond a certain pull-out distance. Thus, in all cases studied in this work, the energy of the fully embedded configuration was lower than the energy of the complete pull-out configuration. As indicated in Figure 5, $E_{pull\text{-}out}$ is the energy difference between the fully embedded configuration of the CNT and the complete pull-out configuration. A similar trend was also observed in previous studies [33,36–38]. Increasing the pull-out displacement, the total potential energy decreased since the interfacial interaction between the CNT and the matrix progressively reduced to zero.

The ISS was calculated from Equation (1), and the results are presented in Figure 6 for all systems. The figures above each column correspond to the number of H-bonds existing at the interface between the CNT and the matrix, and the mean distance (Å) between both structures. The geometrical criteria for the existence of an H-bond are the following: the distance between the H of the donor group (D) and the O of the acceptor group (A) is less than 2.5 Å and the DHA angle is greater than 90°.

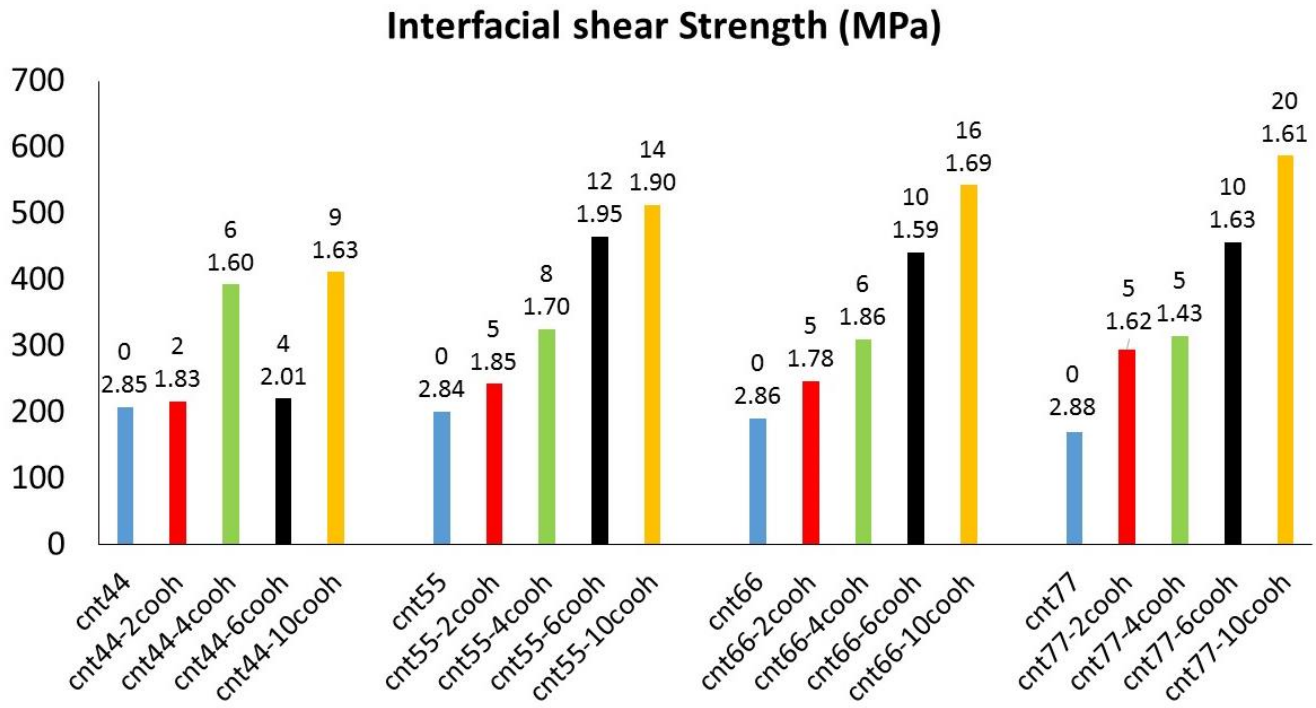

Figure 6. ISS as a function of CNT diameter and number of COOH groups.

It can be seen that ISS values decrease with increasing CNT radius for pristine CNTs. Li et al. [34] found similar results for the pull-out of pristine CNTs from a polyethylene matrix. However, functionalized CNTs do not follow the same trend, and ISS values for these systems seem to be correlated to the number of H-bonds established between the carboxyl groups of the CNT and the tobermorite structure. In general, the higher the number of carboxyl groups, the higher the ISS value. This is because more H-bonds can be formed at the interface, a phenomenon which reinforces the interaction between the CNT and the tobermorite matrix. Some exceptions can be observed. For example, the ISS value for the CNT (4, 4)-4COOH system (392.56 MPa), which presents six H-bonds, is higher than that calculated for the CNT (5, 5)-4COOH system, with eight H-bonds (325.27 MPa). This may be because the mean distance for H-bonds in the CNT (4, 4) system is somewhat smaller (1.60 Å) than that found for the CNT (5, 5) system (1.70 Å), which weakens the interaction.

Some authors analyzed the influence of groups, capable of forming H-bonds with the matrix, on the mechanical properties of graphene-reinforced cementitious composites [37,40,48,60,61]. In all cases, the surface functionalization led to composites with enhanced strength and good binding affinity between the graphene and the cement matrix compared to that of the non-functionalized graphene. In a previous work [62], we also found that the calculated binding energies and experimental results of the mechanical properties of functionalized CNTs are better than those of pristine CNTs. Additionally, other authors found that the functionalized C atoms move out of the nanostructure surface (the hybridization of the functionalized C atom changes from sp^2 to sp^3). The result is that the flat carbon structures turn into wrinkled structures, which mechanically interlock with the matrix, contributing to the enhancement of the mechanical strength [63].

In this work, the calculated ISS values range from 170 to 586 MPa, depending upon the CNT diameter and the number of carboxyl groups bonded to the CNT surface. Other authors found values ranging from 2 to 940 MPa using MD studies of CNT/polymer matrices [64] and references therein]. It would be useful to compare our results with experimental data of single-CNT pull-outs from cement matrices tests. To the best of our knowledge, none are currently available. This may be due to the technical difficulties in designing the experiments and characterizing the interface at the nanoscale. Fan et al. [37] modeled the pull-out of graphene and graphene oxide sheets from a tobermorite crystal,

finding ISS values as high as 647 MPa. Their results are comparable to ours. The ISS values calculated by Alkhateb et al. [38] for pulling-out graphene functionalized with hydroxyl, amine and carboxyl groups varied between 1.2 and 13.5 GPa.

3.2. Non-Bonded Energy

As our models do not include chemical bonds between the CNT and the tobermorite, ISS values can be mainly correlated to changes in non-bonded energy (Van der Waals and electrostatic energies) as the CNT is pulled out from the tobermorite matrix. Figure 7 shows $\Delta E_{\text{non-bonded energy}} = E_{\text{non-bonded energy pulled-out}} - E_{\text{non-bonded energy fully embedded}}$ (non-bonded energy difference between the complete pull-out configuration and the fully embedded configuration of the CNT) for all systems. The higher the value, the stronger the interaction between the CNT and the matrix. Again, the figures above each column correspond to the number of H-bonds existing at the interface between the CNT and the matrix, and the mean distance (Å) between both structures. $\Delta E_{\text{non-bonded energy}}$ follows the same trend as that of ISS. High $\Delta E_{\text{non-bonded energy}}$ values correlate well with the number of H-bonds, indicating a strong interfacial interaction and, therefore, an elevated ISS. The positive correlation between $\Delta E_{\text{non-bonded energy}}$ and ISS is clearly seen in Figure 8. Using MD simulations, Lushnikova et al. [65] inserted a functionalized CNT into a tobermorite structure and found improved bulk modulus, shear modulus, plane stress, and Young's modulus. They attributed the results to the interactions established between the O atoms of the tobermorite and the CNT surface, that is to say, to high non-bonded energy values.

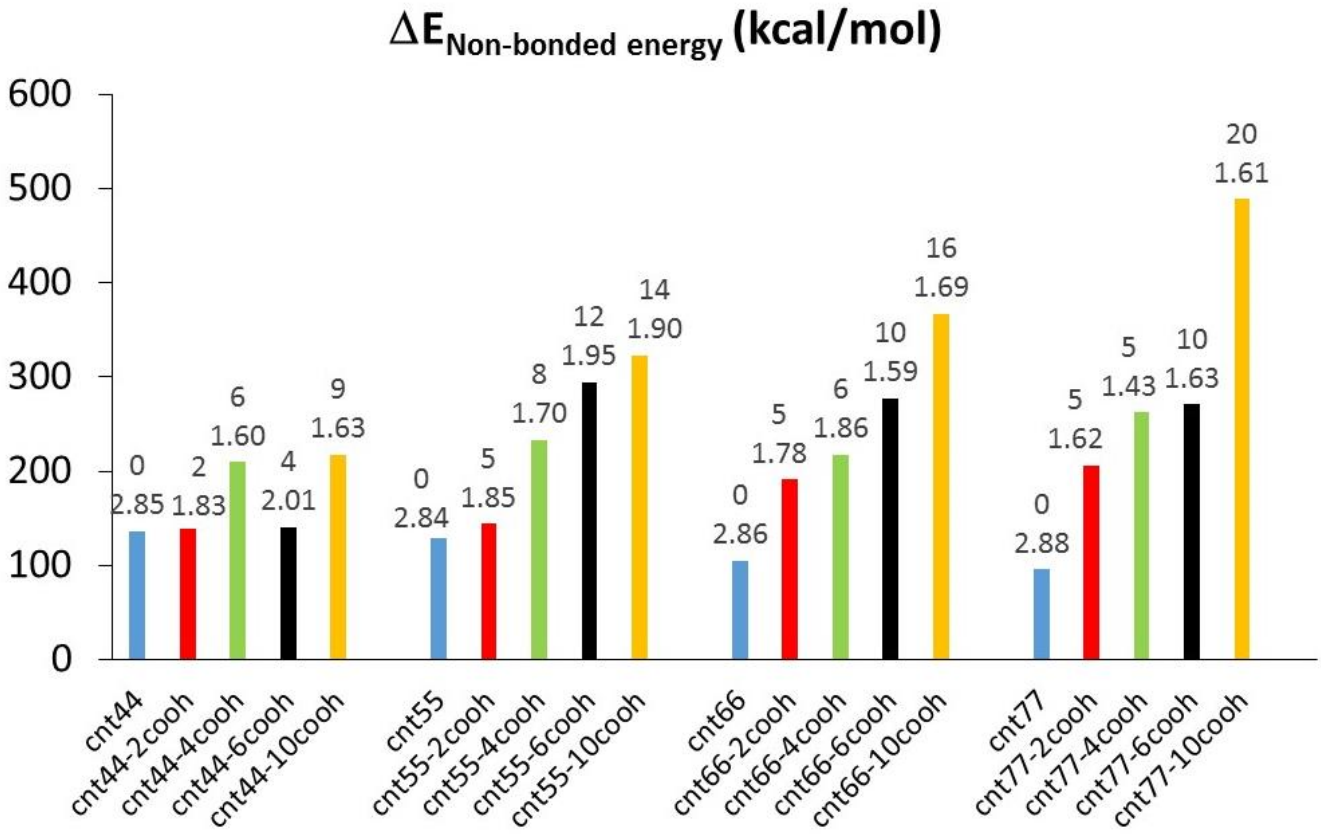

Figure 7. $\Delta E_{\text{non-bonded energy}}$ as a function of CNT diameter and number of COOH groups.

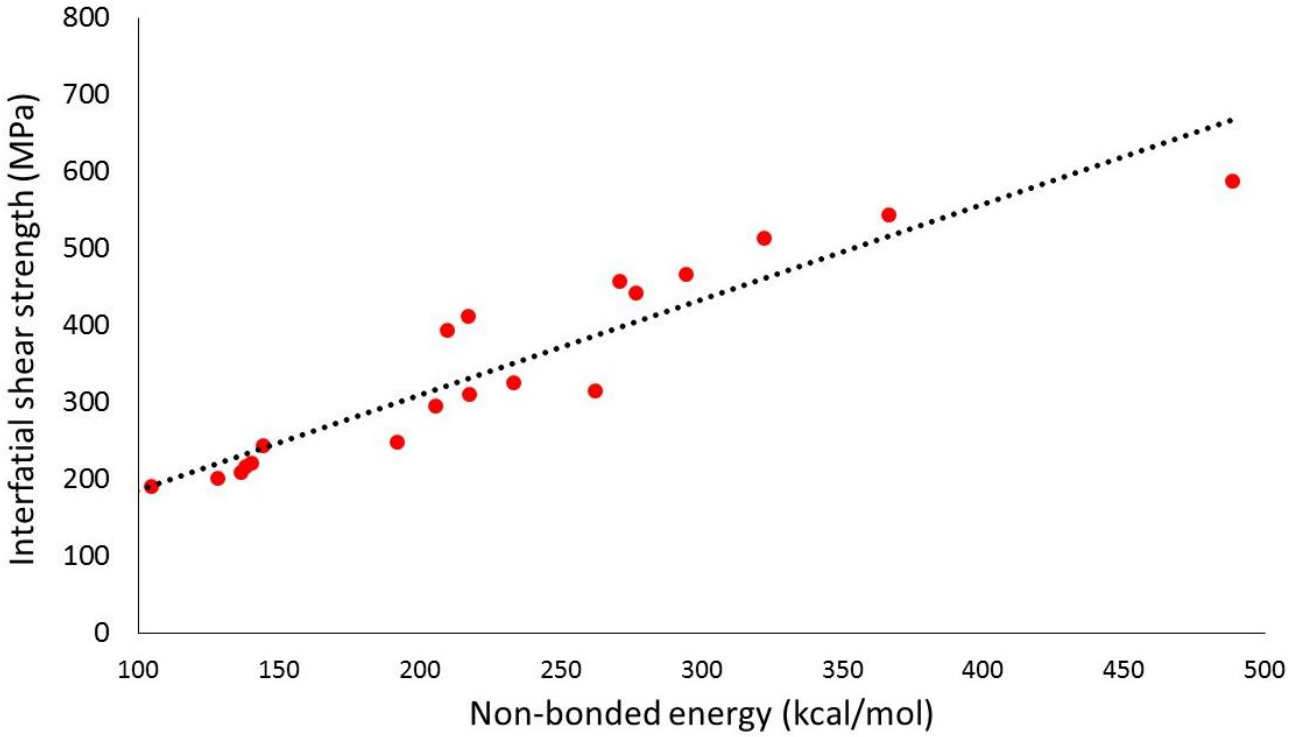

Figure 8. ISS versus $\Delta E_{\text{non-bonded energy}}$.

3.3. Ca^{2+}-O Interactions

Ca^{2+} ions in the tobermorite structure can interact with the functional groups of the CNT, acting as bridges that connect the O atoms of the carboxyl groups with the O atoms of the tobermorite structure. Thus, as in the case of H-bonds, this kind of interaction, mediated by Ca^{2+} ions, improves the adhesion between the CNT and the tobermorite surface. Hou et al. [48] studied the strengthening mechanisms of calcium silicate hydrate (C-S-H) and graphene oxide (GO) using reactive force field molecular dynamics and found that Ca^{2+} ions could bridge O atoms in silicate chains and hydroxyl groups in GO, which resulted in the construction of a reinforcing silicate–carbon skeleton in the interface region. Kai et al. [40] found that the Young's modulus and strength of C-S-H were enhanced by 52.6% and 23.3%, respectively, by the incorporation of hydroxyl groups into the GO. This came because of Ca^{2+} coordination and the formation of hydrogen bonds with the hydroxyl groups of GO. The abovementioned value of 647 MPa, found by Fan et al. [35], is attributed to the strong interactions established between the O atoms of a functionalized GO sheet and the Ca^{2+} ions in the tobermorite structure.

The mean coordination number of Ca^{2+} ions at the interfacial region, the number of Ca^{2+}-carboxylic O close contacts for each CNT, and the mean distance between Ca^{2+} ions and O atoms (either in the carboxyl groups or in the silicate chains) are shown in Table 2 for all systems. As can be seen in Table 2, coordination numbers vary from 5 to 6, with the latter being the preferred one in most structures. It is well known that Ca^{2+} ions in crystal structures generally bind to O atoms in ligands, with coordination numbers mostly ranging from 6 to 8 [66]. Bond lengths are similar to those found in compounds with 6-fold oxygen coordination [67]. In all cases, one or two of the O ligands coordinating a Ca^{2+} ion belong to a carboxyl group of the CNT surface. Furthermore, the number of Ca^{2+} ions that are coordinated by a carboxylic O increases with the number of carboxyl groups, as expected (right column of Table 2). This electrostatic interaction contributes, together with the H-bonds, to the strengthening of the composite interface. The structure of a 6-fold coordinated Ca^{2+} at the interface between the CNT and the tobermorite matrix is shown in Figure 9 for one of the models. For the sake of clarity, some of the atoms of the structure have been removed.

Table 2. Coordination number of Ca^{2+} ions, mean Ca^{2+}-O distance and number of Ca^{2+}-carboxylic O close contacts.

System	Mean Coordination Number	d (Å)	Number of Ca^{2+}-Carboxylic O Close Contacts
cnt44-2cooh	5.0	2.45	2
cnt44-4cooh	5.7	2.53	3
cnt44-6cooh	5.3	2.46	3
cnt44-10cooh	5.3	2.46	4
cnt55-2cooh	5.5	2.34	2
cnt55-4cooh	5.5	2.37	4
cnt55-6cooh	6.0	2.5	5
cnt55-10cooh	6.0	2.47	10
cnt66-2cooh	6.0	2.56	2
cnt66-4cooh	6.0	2.52	4
cnt66-6cooh	6.0	2.48	6
cnt66-10cooh	6.3	2.57	7
cnt77-2cooh	5.5	2.50	2
cnt77-4cooh	5.6	2.45	5
cnt77-6cooh	5.7	2.48	7
cnt77-10cooh	5.9	2.45	8

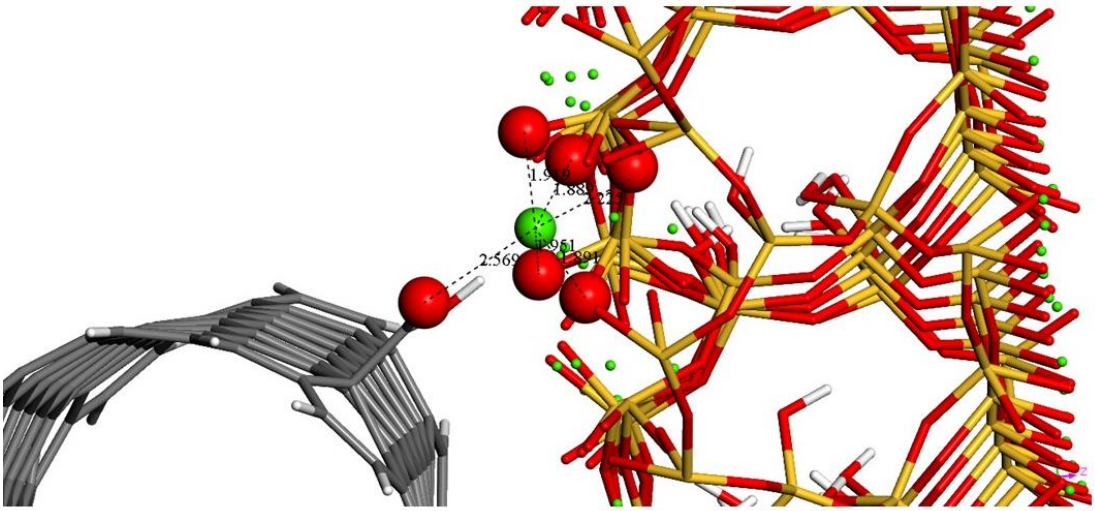

Figure 9. Close look at the interface: 6-fold Ca^{2+} coordination and Ca^{2+}-O bond lengths. Red: oxygen; white: hydrogen; yellow: silicon; grey: carbon; green: calcium.

4. Conclusions

A series of pull-out simulations of pristine and functionalized CNTs, taken from a tobermorite matrix, were carried out to study the interfacial characteristics of the resulting composites. Only non-bonded interactions were considered. The results allow for the following conclusions:

- ISS decreased with increasing CNT radius for pristine CNTs and depended upon the number of H-bonds for functionalized CNTs.
- In the absence of chemical bonds between the CNT and the matrix, ISS values were positively correlated to $\Delta E_{\text{non-bonded energy}}$.
- High, positive $\Delta E_{\text{non-bonded energy}}$ values were mainly derived from the destruction of H-bonds and electrostatic Ca^{2+}-O interactions, as the CNT was pulled out from the

matrix. Specifically, the complete pull-out configuration was less stable than the fully embedded configuration.
- The higher the number of carboxyl groups, the higher the ISS value, as the functionalization of CNTs with these polar groups resulted in both more H-bonds and more Ca^{2+}-O interactions.

Funding: This research received no external funding.

Institutional Review Board Statement: Not applicable.

Informed Consent Statement: Not applicable.

Data Availability Statement: Not applicable.

Conflicts of Interest: The author declares no conflict of interest.

References

1. Reales, O.A.M.; Toledo Filho, R.D. A review on the chemical, mechanical and microstructural characterization of carbon nanotubes-cement based composites. *Constr. Build. Mater.* **2017**, *154*, 697–710. [CrossRef]
2. Shi, T.; Li, Z.; Guo, J.; Gong, H.; Gu, C. Research progress on CNTs/CNFs-modified cement-based composites—A review. *Constr. Build. Mater.* **2019**, *202*, 290–307. [CrossRef]
3. Rocha, V.V.; Ludvig, P.; Trindade, A.C.C.; de Andrade Silva, F. The influence of carbon nanotubes on the fracture energy, flexural and tensile behavior of cement based composites. *Constr. Build. Mater.* **2019**, *209*, 1–8. [CrossRef]
4. Makul, N. Advanced smart concrete—A review of current progress, benefits and challenges. *J. Clean Prod.* **2020**, *274*, 122899. [CrossRef]
5. Metaxa, Z.S.; Tolkou, A.K.; Efstathiou, S.; Rahdar, A.; Favvas, E.P.; Mitropoulos, A.C.; Kyzas, G.Z. Nanomaterials in Cementitious Composites: An Update. *Molecules* **2021**, *26*, 1430. [CrossRef] [PubMed]
6. Li, G.Y.; Wang, P.M.; Zhao, X. Mechanical behavior and microstructure of cement composites incorporating surfacetreated multi-walled carbon nanotubes. *Carbon* **2005**, *43*, 1239–1245. [CrossRef]
7. Li, G.Y.; Wang, P.M.; Zhao, X. Pressure-sensitive properties and microstructure of carbon nanotube reinforced cement composites. *Cem. Concr. Compos.* **2007**, *29*, 377–382. [CrossRef]
8. Gao, F.; Tian, W.; Wang, Z.; Wang, F. Effect of diameter of multi-walled carbon nanotubes on mechanical properties and microstructure of the cement-based materials. *Constr. Build. Mater.* **2020**, *260*, 120452. [CrossRef]
9. Gao, Y.; Jing, H.; Zhou, Z.; Shi, X.; Li, L.; Fu, G. Roles of carbon nanotubes in reinforcing the interfacial transition zone and impermeability of concrete under different water-to-cement ratios. *Constr. Build. Mater.* **2021**, *272*, 121664. [CrossRef]
10. Adhikary, S.K.; Rudžionis, Z.; Rajapriya, R. The Effect of carbon nanotubes on the flowability, mechanical, microstructural and durability properties of cementitious composite: An overview. *Sustainability* **2020**, *12*, 8362. [CrossRef]
11. Du, Y.; Gao, P.; Yang, J.; Shi, F.; Shabaz, M. Experimental Analysis of Mechanical Properties and Durability of Cement-Based Composite with Carbon Nanotube. *Adv. Mater. Sci. Eng.* **2021**, *2021*, 8777613. [CrossRef]
12. Silvestro, L.; Ruviaro, A.; Lima, G.; de Matos, P.; de Azevedo, A.R.G.; Monteiro, S.N.; Gleize, P. Influence of Ultrasonication of Functionalized Carbon Nanotubes on the Rheology, Hydration, and Compressive Strength of Portland Cement Pastes. *Materials* **2021**, *14*, 5248. [CrossRef] [PubMed]
13. Jongvivatsakul, P.; Thongchom, C.; Mathuros, A.; Prasertsri, T.; Adamu, M.; Orasutthikul, S.; Lenwari, A.; Charainpanitkul, T. Enhancing bonding behavior between carbon fiber-reinforced polymer plates and concrete using carbon nanotube reinforced epoxy composites. *Case Stud. Constr. Mater.* **2022**, *17*, e01407. [CrossRef]
14. Yu, Z.; Lau, D. Evaluation on mechanical enhancement and fire resistance of carbon nanotube (CNT) reinforced concrete. *Coupled Syst. Mech.* **2017**, *6*, 335–349.
15. Qin, R.; Zhou, A.; Yu, Z.; Wang, Q.; Lau, D. Role of carbon nanotube in reinforcing cementitious materials: An experimental and coarse-grained molecular dynamics study. *Cem. Concr. Res.* **2021**, *147*, 106517. [CrossRef]
16. Sindu, B.S.; Sasmal, S. Molecular dynamics simulations for evaluation of surfactant compatibility and mechanical characteristics of carbon nanotubes incorporated cementitious composite. *Constr. Build. Mater.* **2020**, *253*, 119190.
17. Balasubramaniam, B.; Mondal, K.; Ramasamy, K.; Palani, G.S.; Iyer, N.R. Hydration Phenomena of Functionalized Carbon Nanotubes (CNT)/Cement Composites. *Fibers* **2017**, *5*, 39. [CrossRef]
18. Sarvandani, M.M.; Mahdikhani, M.; Aghabarati, H.; Fatmehsari, M.H. Effect of functionalized multi-walled carbon nanotubes on mechanical properties and durability of cement mortars. *J. Build. Eng.* **2021**, *41*, 102407. [CrossRef]
19. Balasubramanian, K.; Burghard, M. Chemically functionalized carbon nanotubes. *Small* **2005**, *1*, 180–192. [CrossRef]
20. Mallakpour, S.; Soltaniana, S. Surface functionalization of carbon nanotubes: Fabrication and applications. *RSC Adv.* **2016**, *6*, 109916. [CrossRef]
21. Liu, P. Modifications of carbon nanotubes with polymer. *Eur. Polym. J.* **2005**, *41*, 2693–2703. [CrossRef]

22. Peng, H.; Alemany, L.B.; Margrave, J.L.; Khabashesku, V.N. Sidewall Carboxylic Acid Functionalization of Single-Walled Carbon Nanotubes. *J. Am. Chem. Soc.* **2003**, *125*, 15174–15182. [CrossRef] [PubMed]
23. Kang, S.T.; Seo, J.Y.; Park, S.H. The Characteristics of CNT/Cement Composites with Acid-Treated MWCNTs. *Adv. Mater. Sci. Eng.* **2015**, *2015*, 308725. [CrossRef]
24. Ruan, Y.; Han, B.; Yu, X.; Zhang, W.; Wang, D. Carbon nanotubes reinforced reactive powder concrete. *Compos. Part A Appl. Sci. Manuf.* **2018**, *112*, 371–382. [CrossRef]
25. Yilmaz, Y.L. Analyzing single fiber fragmentation test data by using stress transfer model. *J. Compos. Mater.* **2002**, *36*, 537–551. [CrossRef]
26. Zhao, Y.R.; Xing, Y.M.; Lei, Z.K. Interfacial stress transfer behavior in a specially-shaped fiber/matrix pullout test. *Acta Mech. Sin.* **2010**, *26*, 113–119. [CrossRef]
27. Zu, M.; Li, Q.; Zhu, Y. The effective interfacial shear strength of carbon nanotube fibers in an epoxy matrix characterized by a microdroplet test. *Carbon* **2012**, *50*, 1271–1279. [CrossRef]
28. Battisti, A.; Esqué-de los Ojos, D.; Ghisleni, R. Single fiber push-out characterization of interfacial properties of hierarchical CNT-carbon fiber composites prepared by electrophoretic deposition. *Compos. Sci. Technol.* **2014**, *95*, 121–127. [CrossRef]
29. Rodríguez, M.; Molina-Aldareguía, J.M.; González, C. A methodology to measure the interface shear strength by means of the fiber push-in test. *Compos. Sci. Technol.* **2012**, *72*, 1924–1932. [CrossRef]
30. Ji-Hong, J.; Chan, Y.; Chan-Gi, P. Bonding Characteristics of Macrosynthetic Fiber in Latex-Modified Fiber-Reinforced Cement Composites as a Function of Carbon Nanotube Content. *Int. J. Polym. Sci.* **2016**, *2016*, 7324975.
31. Li, Y.; Wang, Q.; Wang, S. A review on enhancement of mechanical and tribological properties of polymer composites reinforced by carbon nanotubes and graphene sheet: Molecular dynamics simulations. *Compos. B Eng.* **2019**, *160*, 348–361. [CrossRef]
32. Liao, K.; Li, S. Interfacial characteristics of a carbon nanotube–polystyrene composite system. *Appl. Phys. Lett.* **2001**, *79*, 4225. [CrossRef]
33. Chowdhury, S.C.; Okabe, T. Computer simulation of carbon nanotube pull-out from polymer by the molecular dynamics method. *Compos. Part A Appl. Sci. Manuf.* **2007**, *38*, 747–754. [CrossRef]
34. Li, Y.; Liu, Y.; Peng, X.; Yan, C.; Liu, S.; Hu, N. Pull-out simulations on interfacial properties of carbon nanotube-reinforced polymer nanocomposites. *Comput. Mater. Sci.* **2011**, *50*, 1854–1860. [CrossRef]
35. Chandra, Y.; Scarpa, F.; Adhikari, S.; Zhang, J.; Flores, E.S.; Peng, H.X. Pullout strength of graphene and carbon nanotube/epoxy composites. *Compos. B Eng.* **2016**, *102*, 1–8. [CrossRef]
36. Chawla, R.; Sharma, S. Molecular dynamics simulation of carbon nanotube pull-out from polyethylene matrix. *Compos. Sci. Technol.* **2017**, *144*, 169–177. [CrossRef]
37. Fan, D.; Lue, L.; Yang, S. Molecular dynamics study of interfacial stress transfer in graphene-oxide cementitious composites. *Comput. Mater. Sci.* **2017**, *139*, 56–64. [CrossRef]
38. Alkhateb, H.; Al-Ostaz, A.; Cheng, A.H.D.; Li, X. Materials genome for graphene-cement nanocomposites. *J. Nanomechanics Micromechanics* **2013**, *3*, 67–77. [CrossRef]
39. Eftekhari, M.; Mohammadi, S. Molecular dynamics simulation of the nonlinear behavior of theCNT-reinforced calcium silicate hydrate (C–S–H) composite. *Int. J. Impact. Eng.* **2016**, *82*, 78–87.
40. Kai, M.; Zhang, L.; Liew, K. Graphene and graphene oxide in calcium silicate hydrates: Chemical reactions, mechanical behaviors and interfacial sliding. *Carbon* **2019**, *146*, 181–193. [CrossRef]
41. Lv, C.; Xue, Q.; Xia, D.; Ma, M.; Xie, J.; Chen, H. Effect of chemisorption on the interfacial bonding characteristics of graphene−polymer composites. *J. Phys. Chem. C* **2010**, *114*, 6588–6594. [CrossRef]
42. Shiu, S.C.; Tsai, J.L. Characterizing thermal and mechanical properties of graphene/ epoxy nanocomposites. *Compos. B Eng.* **2014**, *56*, 691–697. [CrossRef]
43. Li, Y.; Wang, S.; Wang, Q. Enhancement of tribological properties of polymer composites reinforced by functionalized graphene. *Compos. B Eng.* **2017**, *120*, 83–91. [CrossRef]
44. Nikkhah, S.J.; Moghbeli, M.R.; Hashemianzadeh, S.M. Investigation of the interface polyethylene and functionalized graphene: A computer simulation study. *Curr. Appl. Phys.* **2015**, *15*, 1188–1199. [CrossRef]
45. Zhang, J.; Jiang, D. Molecular dynamics simulation of mechanical performance of graphene/graphene oxide paper based polymer composites. *Carbon* **2014**, *67*, 784–791. [CrossRef]
46. Bauchy, M.; Qomi, M.A.; Ulm, F.J.; Pellenq, R.M. Order and Disorder in Calcium-silicate-hydrate. *J. Chem. Phys.* **2014**, *140*, 214503. [CrossRef]
47. Richardson, I.G. Tobermorite/jennite- and tobermorite/calcium hydroxide-based models for the structure of C–S–H: Applicability to hardened pastes of tricalcium silicate, -dicalcium silicate, Portland cement, and of Portland cement with blast-furnace slag, metakaolin, or silica fume. *Cem. Concr. Res.* **2004**, *34*, 1733–1777.
48. Hou, D.; Lu, Z.; Li, X.; Ma, H.; Li, Z. Reactive molecular dynamics and experimental study of graphene-cement composites: Structure, dynamics and reinforcement mechanisms. *Carbon* **2017**, *115*, 188–208. [CrossRef]
49. Allen, A.J.; Thomas, J.J.; Jennings, H.M. Composition and density of nanoscale calcium–silicate–hydrate in cement. *Nat. Mater.* **2007**, *6*, 311–316. [CrossRef]
50. Hoover, W.G. Canonical dynamics: Equilibrium phase-space distributions. *Phys. Rev. A* **1985**, *31*, 1695–1697. [CrossRef]

51. Berendsen, H.J.C.; Postma, J.P.M.; Van Gunsteren, W.F.; DiNola, A.; Haak, J.R. Molecular dynamics with coupling to an external bath. *J. Chem. Phys.* **1984**, *81*, 3684–3690. [CrossRef]
52. Materials Studio Materials Modeling & Simulation Application | Dassault Systèmes BIOVIA. Available online: https://www.3ds.com/products-services/biovia/products/molecular-modeling-simulation/biovia-materials-studio/ (accessed on 21 November 2022).
53. Sun, H.; Ren, P.; Fried, J.R. The COMPASS force field: Parameterization and validation for phosphazenes. *Comput. Theor. Polym. Sci.* **1998**, *8*, 229–246. [CrossRef]
54. Bhuvaneshwari, B.; Palani, G.S.; Karunya, R.; Iyer, N.R. Nano mechanical properties on the mineralogical array of calcium silicate hydrates and calcium hydroxide through molecular dynamics-CSIR-SERC. *Curr. Sci.* **2015**, *108*, 1058–1065.
55. Du, J.; Bu, Y.; Shen, Z. Interfacial properties and nanostructural characteristics of epoxy resin in cement matrix. *Constr. Build. Mater.* **2018**, *164*, 103–112. [CrossRef]
56. Al-Ostaz, A.; Wu, W.; Cheng, A.-D.; Song, C. A molecular dynamics and microporomechanics study on the mechanical properties of major constituents of hydrated cement. *Compos. Part B Eng.* **2010**, *41*, 543–549. [CrossRef]
57. Hajilar, S.; Shafei, B. Nano-scale investigation of elastic properties of hydrated cement paste constituents using molecular dynamics simulations. *Comput. Mater. Sci.* **2015**, *101*, 216–226. [CrossRef]
58. Tosi, M. Cohesion of ionic solids in the Born model. In *Solid State Physics*; Elsevier: Amsterdam, The Netherlands, 1964; Volume 16, pp. 1–120.
59. Gou, J.; Minaie, B.; Wang, B.; Liang, Z.; Zhang, C. Computational and experimental study of interfacial bonding of single-walled nanotube reinforced composites. *Comput. Mater. Sci.* **2004**, *31*, 225–236. [CrossRef]
60. Al-Muhit, B.; Sanchez, F. Nano-engineering of the mechanical properties of tobermorite 14 Å with graphene via molecular dynamics simulations. *Constr. Build. Mater.* **2020**, *233*, 117237. [CrossRef]
61. Sanchez, F.; Zhang, L. Molecular dynamics modeling of the interface between surface functionalized graphitic structures and calcium–silicate–hydrate: Interaction energies, structure, and dynamics. *J. Colloid. Interface Sci.* **2008**, *323*, 349–358. [CrossRef]
62. Merodio-Perea, R.G.; Páez-Pavón, A.; Lado-Touriño, I. Reinforcing cement with pristine and functionalized carbon nanotubes: Experimental and simulation studies. *Int. J. Smart Nano Mater.* **2020**, *11*, 370–386. [CrossRef]
63. Wang, M.C.; Lai, Z.B.; Galpaya, D.; Yan, C.; Hu, N.; Zhou, L.M. Atomistic simulation of surface functionalization on the interfacial properties of graphene-polymer nanocomposites. *J. Appl. Phys.* **2014**, *115*, 123520. [CrossRef]
64. Mani, A.; Sharma, S. Interfacial shear strength of carbon nanotube reinforced polymer composites: A review. *Mater. Today Proc.* **2022**, *50*, 1774–1780. [CrossRef]
65. Lushnikova, A.; Zaoui, A. Improving mechanical properties of C–S–H from inserted carbon nanotubes. *J. Phys. Chem. Solids* **2017**, *105*, 72–80. [CrossRef]
66. Katz, A.K.; Glusker, J.P.; Beebe, S.A.; Bock, C.W. Calcium Ion Coordination: A CoMParison with That of Beryllium, Magnesium, and Zinc. *J. Am. Chem. Soc.* **1996**, *118*, 5752–5763. [CrossRef]
67. Sowrey, F.E.; Skipper, L.J.; Pickup, D.M.; Drake, K.O.; Lin, Z.; Smith, M.E.; Newport, R.J. Systematic empirical analysis of calcium–oxygen coordination environment by calcium K-edge XANES. *Phys. Chem. Chem. Phys.* **2004**, *6*, 188–192. [CrossRef]